MRI-Based Computational Fluid Dynamics in Experimental Vascular Models: Toward the Development of an Approach for Prediction of Cardiovascular Changes During Prolonged Space Missions

T. A. Spirka[1], J. G. Myers[2], R. M. Setser[3], S. S. Halliburton[3], R. D. White[3], G. P. Chatzimavroudis[1,3]

[1]Chemical and Biomedical Engineering, Cleveland State University, Cleveland, OH, United States, [2]Human Health and Performance Systems Projects Office - Exploration Systems Division, NASA - Glenn Research Center, Cleveland, OH, United States, [3]Radiology, The Cleveland Clinic Foundation, Cleveland, OH, United States

Introduction and Aim: A priority of NASA is to identify and study possible risks to astronauts' health during prolonged space missions [1]. The goal is to develop a procedure for a preflight evaluation of the cardiovascular system of an astronaut and to forecast how it will be affected during the mission. To predict these changes, a computational cardiovascular model must be constructed. Although physiology data can be used to make a general model, a more-desirable subject-specific model requires anatomical, functional, and flow data from the specific astronaut. MRI has the unique advantage of providing images with all of the above information, including three-directional velocity data which can be used as boundary conditions in a computational fluid dynamics (CFD) program [2,3]. MRI-based CFD is very promising for reproduction of the flow patterns of a specific subject and prediction of changes in the absence of gravity. The aim of this study was to test the feasibility of this approach by reconstructing the geometry of MRI-scanned arterial models and reproducing the MRI-measured velocities using CFD simulations on these geometries.

Methods: An aortic glass model and a carotid glass model were used for the MRI experiments (Figs.1 and 2). The aortic model consisted of the ascending and descending aorta, and a non-planar (20° out of plane) arch between them. The carotid model consisted of the common, internal (with the bulb), and external carotid arteries with a planar bifurcation. Both models were scanned using a 1.5T MRI scanner (Siemens Sonata). Scanning consisted of two parts. In the first part, a number of contiguous gradient-echo (slice thickness: combination of 3 and 5 mm; FOV: 256×256 mm^2) images was acquired perpendicular to the axis of the vessel. In the arch, the slices were contiguous along the inner curve. Two matrix sizes (256x256 and 512x512) provided a lower and a higher resolution set. In the second part, three-directional MR phase velocity mapping was performed with 3 mm thick slices (FOV: 256x256 mm^2, TE: 3-6 ms; Venc: 30 cm/s) placed perpendicular to the vessel axis at the locations shown in Fig.1 and along the vessel axis (Fig.2). Steady flow experiments were performed (aortic: 1.7 and 3.0 L/min; carotid: 0.9 and 1.8 L/min). The geometry images were segmented using ImageJ (NIH) and the models were reconstructed using Rhinoceros (Robert McNeel & Associates), before being imported into CFD-GEOM (CFD Research Corporation) for meshing. The computation was performed using CFD-ACE (CFD Research Corporation). The phase (velocity) images were processed using Transform (Research Systems, Inc.). These velocity data provided the 2D inlet velocity boundary conditions (slice 1, Fig.1a and Fig.1b) and the reference data (rest of slices) for the evaluation of the CFD results.

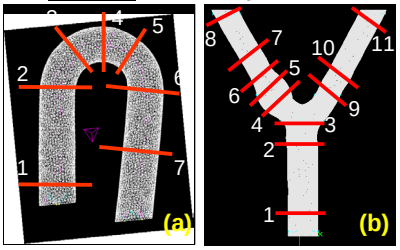

Fig.1: The aortic arch (a) and carotid bifurcation (b) models and the locations for the axial velocity measurements

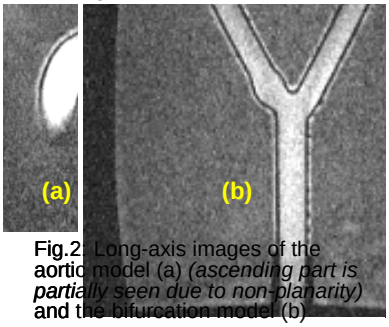

Fig.2 Long-axis images of the aortic model (a) *(ascending part is partially seen due to non-planarity)* and the bifurcation model (b)

Results and Discussion: The MRI-measured flow rates (calculated by integrating the velocity over the cross-sectional area) and the CFD flow rates showed close agreement (differences <5%) throughout the models. Contour and vector plots of the velocity were created using the MRI velocity data and the CFD data. Fig.3 shows the left-to-right MRI-measured (left) and CFD-calculated (right) velocity component in the aortic arch model, revealing qualitative and quantitative agreement (local differences <15%). Fig.4 shows the MRI (left) and CFD (right) through-plane velocity at the top of the arch. The inner wall of the curve is on the left of the cross-sections where the velocity is lower due to the curvature. Again, close agreement (local differences <10%) was found between the MRI and CFD results with a peak velocity approximately 15 cm/s. In-plane vector plots at the same location showed a single vortex formation (with only traces of a second vortex), instead of the two vortices seen in Dean's curved flow, probably due to the non-planarity of the arch. Fig.5 displays the MRI (left) and CFD (right) vector plots in the bifurcation model, showing identical flow patterns in all vessels and in the bulb (high velocities along the inner wall and low velocities along the outer wall with flow reversal). The vector plots at the end of the bulb (slice 6, Fig.1b), as shown in Fig.6, display a formation of a double vortex as a result of the curvature from the parent to the branch vessels. In all cases, the CFD velocity results agreed well (average local differences of <20%) with the MRI-measured velocity data which were used as the reference data in order to evaluate the accuracy of the CFD results. Fig.7 shows specifically the CFD and MRI velocity profiles in the bulb (slice 5, Fig.1b). The profiles are skewed, as expected, with high velocities near the inner wall and low velocities (and some flow reversal) near the outer wall. The differences between the MRI and CFD high velocity regions (close to inner wall) were <20% in all slice locations. The resolution of the geometric MRI acquisitions (used to make the computational models) did not affect the CFD results (<5% differences in the CFD results between the 256x256 and 512x512 matrix sizes).

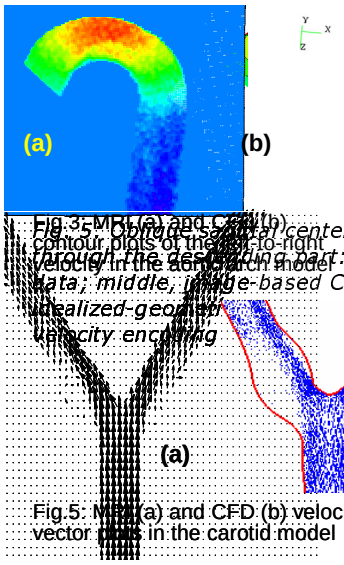

Fig.3: MRI (a) and CFD (b) contour plots of the left-to-right velocity in the aortic arch model

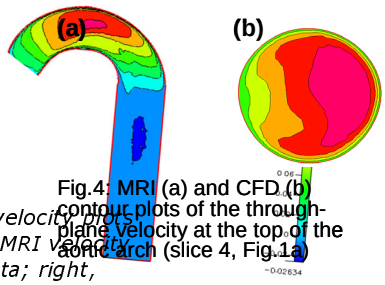

Fig.4: MRI (a) and CFD (b) contour plots of the through-plane velocity at the top of the aortic arch (slice 4, Fig.1a)

Fig.5: Oblique sagittal centerline velocity plots through the descending part: left, MRI velocity data; middle, image-based CFD data; right, idealized-geometry CFD data. The figure shows the velocity encoding

Fig.5: MRI (a) and CFD (b) velocity vector plots in the carotid model

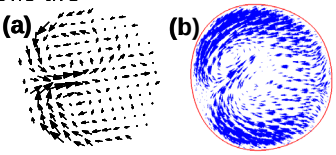

Fig.6: MRI (a) and CFD (b) in-plane velocity vector plots in the carotid model (slice 6, Fig.1b)

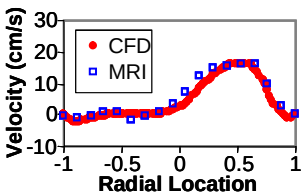

Fig.7: CFD and MRI centerline velocity profiles in the bulb of the bifurcation (slice 5, Fig.1b)

Conclusion: The results from this study show that image-based CFD simulations provide reliable velocity characterization and quantification in arterial models. These results are the first step toward the construction of a subject-specific model of the cardiovascular system, based on a full-scale MRI acquisition of the anatomy, composition, function, and blood velocity (the latter for the boundary condition) of the heart and vascular tree, able to predict functional and flow changes due to variation of external parameters, such as gravity.

References: *[1] White RJ et al., Adv Space Res 31:7-16 (2003); [2] Steinman DA, Ann Biom Eng 30:483-497 (2002); [3] Zhao SZ, Ann Biom Eng 31:962-971 (2003)*